Available online at www.sciencedirect.com
SCIENCE DIRECT
ELSEVIER
European Journal of Mechanics B/Fluids 25 (2006) 279–301
EUROPEAN JOURNAL OF MECHANICS B/FLUIDS

Upstream nozzle shaping effects on near field flow in round turbulent free jets

W.R. Quinn

Department of Engineering, St. Francis Xavier University, Antigonish, Nova Scotia, Canada B2G 2W5

Received 23 December 2004; received in revised form 7 October 2005; accepted 27 October 2005

Available online 2 December 2005

Abstract

Isothermal, incompressible round turbulent free jets of air, issuing from a sharp-edged orifice and from a contoured nozzle into still air surroundings, have been used to study the effects of upstream nozzle shaping on near field jet evolution experimentally. The Reynolds number, based on the diameter of the orifice or the nozzle, was 1.84×10^5 in both jets. Hot-wire anemometry and a pitot-static tube were used to obtain the measured quantities which included the mean streamwise velocity, the turbulent Reynolds normal and shear stresses, the autocorrelation coefficients and one-dimensional energy spectra of the fluctuating streamwise velocity and the mean static pressure. The mean streamwise velocity decay on the jet centerline and the jet half-velocity widths were obtained from the mean streamwise velocity data. To the extent that the results showed that mixing in the sharp-edged orifice round jet was higher than in the contoured nozzle round jet, upstream nozzle shaping was found to affect jet evolution in the near flow field. The distribution of the autocorrelation coefficients of the streamwise fluctuating velocity showed a marked difference in the evolution of the two jets, one of which had a uniform, and the other a non-uniform, exit plane mean streamwise velocity profile. The one-dimensional energy spectra results and also those of the distribution of the autocorrelation coefficients indicated the presence of coherent structures in the near field of the jets and the sharp-edged orifice jet was found to be more "energetic" than the contoured nozzle jet.

Keywords: Jets; Nozzles; Mixing; Turbulence

1. Introduction

The round geometry, because of the ease with which it can be produced, is found in many applications in engineering. Jets which issue from round nozzles into essentially unbounded surroundings are useful in a number of areas of technical interest. This jet flow configuration has, consequently, been and continues to be the subject of many contributions to basic fluid mechanics research. A round jet can emanate from a pipe, from a nozzle with smoothly contracting shaping upstream of the nozzle exit plane or from a sharp-edged orifice. These three different exit conditions lead, of course, to different developments of the flow downstream of the nozzle or orifice exit plane. Depending upon the requirements of the applications in which the jets are used, one or the other of the three exit conditions mentioned previously may be used. Regardless of the exit shape used, the flow field of a round jet can be divided into

E-mail address: wquinn@stfx.ca (W.R. Quinn).

0997-7546/$ – see front matter
doi:10.1016/j.euromechflu.2005.10.002

three regions, namely, an initial or flow development region, referred to as the potential core when the exit velocity profile is top hat, a transition region and a fully developed region. Detailed experimental studies of the fully developed region have been carried out by Wygnanski and Fiedler [1] and by Rodi [2], among others, and, more recently, by Panchapakesan and Lumley [3]. The mean flow and turbulence quantities show self-similar distributions in the fully developed region and this has facilitated the analytic treatment of the jet in this region. Such analyses can be found, for example, in Rajaratnam [4] and in Schlichting [5]. The near and transition regions of the jet have been studied by Sami et al. [6], Hill [7], Boguslawski and Popiel [8] and Obot et al. [9], among others. The study of Sami et al. [6] presented mean flow, mean static pressure and turbulence data for a round jet issuing from a smoothly contoured nozzle. Mass entrainment data for the flow of a round jet issuing from a short converging nozzle were provided by the study of Hill [7]. The round jet issuing from a long circular pipe, with a fully developed turbulent velocity profile, was studied by Boguslawski and Popiel [8] and the study contributed mean flow and turbulence data. Mean streamwise velocity data, from which the spreading and entrainment rates in a jet issuing from a square-edged orifice were obtained, were provided by the study of Obot et al. [9].

The effects of nozzle upstream shaping or initial conditions on the downstream development of round jets have not been totally ignored in the extant literature. The important role played by the initial conditions in the spatial and temporal evolution of jets has indeed been recognized for some time now. Quinn and Militzer [10], in an experimental and numerical study of the near flow field of round jets issuing from a sharp-edged orifice and from a contoured nozzle, have shown by means of mean flow and time-averaged turbulence and mean static pressure data that mixing is higher in a sharp-edged orifice jet than in a contoured nozzle jet. Mi et al. [11] did a comparative study of mixing in round jets issuing from a contoured nozzle, an orifice plate and a pipe and concluded, by means of flow visualization, mean and time-averaged fluctuating temperature data and one-dimensional energy spectra of the fluctuating streamwise velocity, that the highest mixing occurs in the orifice plate jet and that the mixing in the contoured nozzle jet is, in turn, higher than that in the pipe jet.

It is noteworthy that the data in all of the aforementioned studies were acquired along lines of symmetry and were presented as profiles. While information contained in such profiles is useful and has contributed to the knowledge base on round jets, more complete information about the evolution of the jet can be obtained from data acquired across entire planes at selected streamwise locations. The present study was undertaken to extend the scope of the experimental part of the work reported in Quinn and Militzer [10]. The objective was to determine the effects of the upstream shaping of the nozzle, namely, sharp-edged orifice versus contoured nozzle, on the downstream development of round turbulent free jets in the near flow field. The data, obtained across entire streamwise planes, used to achieve the stated objective of the study include the mean streamwise velocity, the mean static pressure, time-averaged turbulence statistics and the autocorrelations and one-dimensional spectra of the streamwise fluctuating velocity. The jet half-velocity widths and the mean streamwise velocity decay on the jet centerline have been obtained from the mean streamwise velocity data and are used to assess mixing in the two jets.

2. Experimental details

The jet flow facility used for the present study is shown in Fig. 1. It consists of a small centrifugal fan, a diffuser, a settling chamber, a three-dimensional contraction and a screen cage. The fan, which drew air from a room adjacent to the laboratory and delivered it to the sharp-edged orifice or contoured nozzle via the diffuser, settling chamber and contraction, was supported on anti-vibration neoprene pads. The diffuser was fitted with a baffle at its upstream end, honeycomb and mesh-wire screens. The settling chamber, a plywood box, of 0.762 m $\times$ 0.762 m cross-section and 1.054 m in length, was also fitted with mesh-wire screens. The three-dimensional contraction had a contour which is a third-degree polynomial that had zero derivatives as end conditions. The contraction, 0.523 m in length, had a circular cross-section, with 0.762 m diameter at its upstream end, and a 0.305 m $\times$ 0.305 m square cross-section at its downstream end. The sharp-edged orifice, which is shown in Fig. 2, or the contoured nozzle, which is shown in Fig. 3, capped the downstream end of the contraction, which was flush with a 2.438 m $\times$ 2.438 m plywood wall. The Cartesian coordinate system used is shown in Fig. 2. The streamwise (X) coordinate is perpendicular to the spanwise (Y) and lateral (Z) coordinates and forms a right-hand system with them. The contraction ratio was 283. The plywood wall formed one side of a screen cage which extended 3.658 m downstream from the wall. The experiments were performed in a 7.70 m $\times$ 7.01 m $\times$ 2.87 m room.

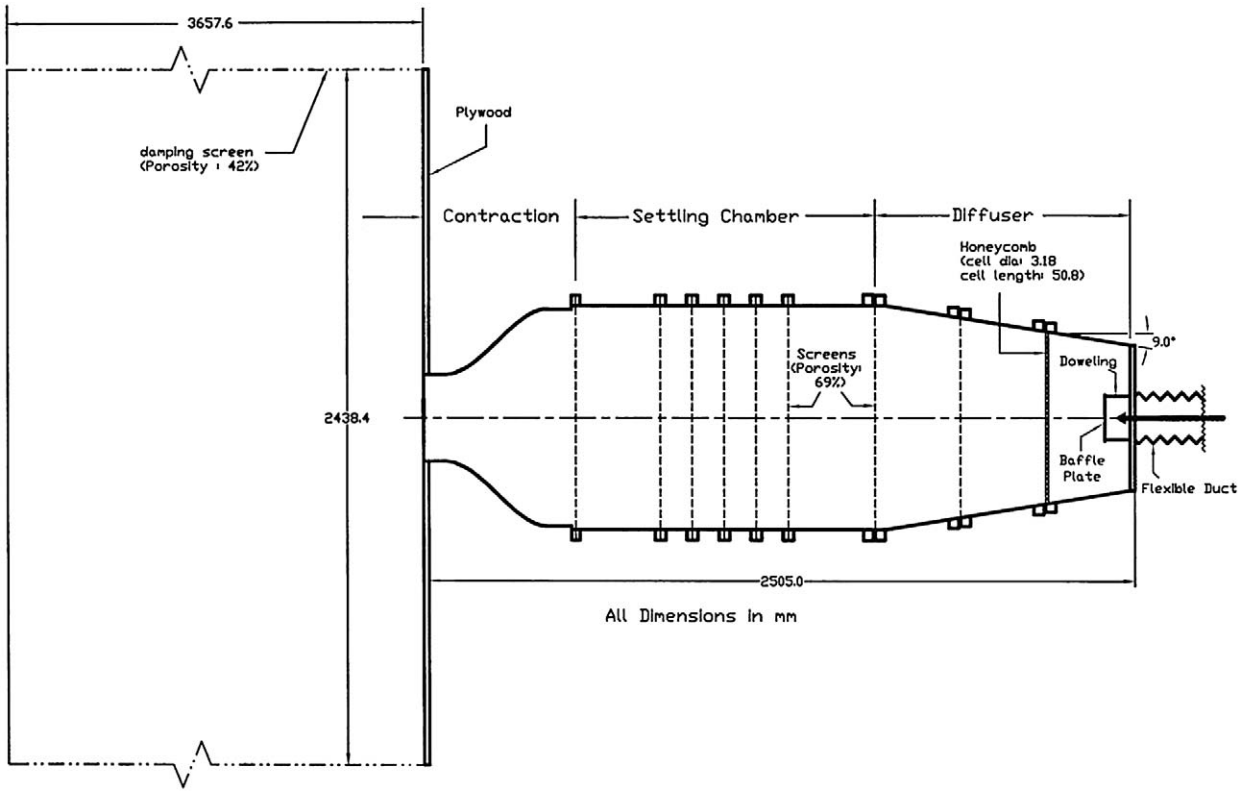

Fig. 1. Plan view section of the flow facility.

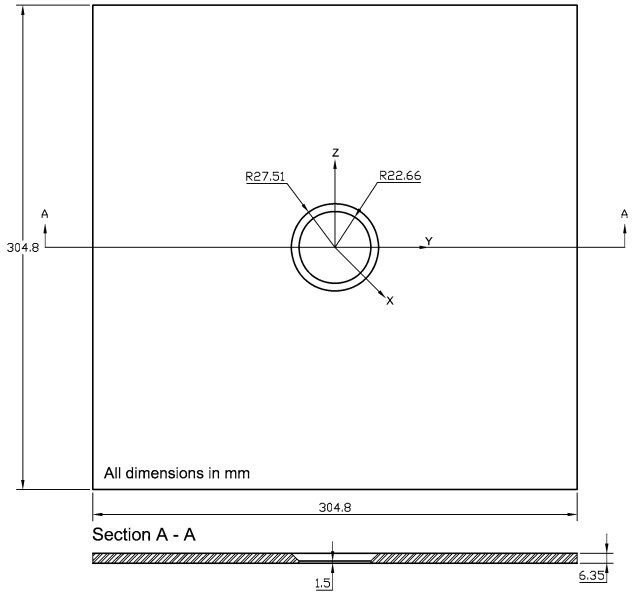

Fig. 2. Sharp-edged orifice.

A three-dimensional traversing system was used for moving the sensing probes in the flow field. The system consisted of a rack and pinion for traversing in the X direction and lead screws for traversing in the Y and Z directions. The base of the traversing system was, like the fan, also supported on anti-vibration neoprene pads. Traversing in all

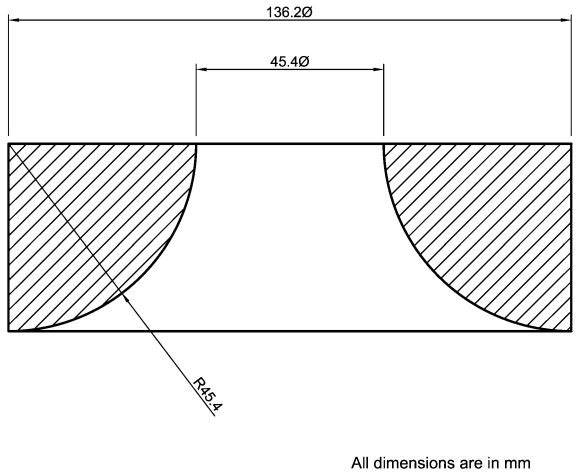

Fig. 3. Contoured nozzle.

three coordinate directions was effected by microcomputer-controlled stepping motors. Positioning accuracy of the sensing probes was 0.3 mm in the X direction and 0.01 mm in both the Y and Z directions. The data were acquired on a grid, in the Y–Z plane, at each X location. The grid spacing, which was kept the same in the Y and Z directions, varied from 2.54 mm close to the jet exit to 12.7 mm further downstream.

The mean velocity and turbulence data were acquired with DANTEC P51 X-array probes. These probes consist of two 5 μm diameter platinum-plated tungsten slant wire sensing elements about 1 mm long and about 1 mm apart. The hot-wire probes, operated by DANTEC constant temperature anemometers at a resistance ratio of 1.8, were calibrated on-line close to the exit of the jet against the output of a pitot-static tube which was connected to a pressure transducer and a Barocel electronic manometer. The calibration data were fitted to the exponent power law: $E^2 = A + BU_{\text{eff}}^n$ and A, B and n were optimized with a linear least-squares goodness-of-fit procedure. This procedure involved using various values of n until the square of the "fitting" error was at a minimum. The resulting values of A, B and n were then taken as the optimum values. E is the hot-wire output voltage and A, B and n are constants. A "cosine law" response to yaw was assumed and the effective angle was found from a yaw calibration following the procedure described in Bradshaw [12]. Temperature variations from the calibration temperature were monitored with a thermocouple placed in close proximity to the hot-wire probe and corrections for such variations were made using the procedure in Bearman [13] in the data-reduction software. The mean flow and turbulence data were corrected for the effects of the mean velocity gradients on the spacing between the two slant sensing-wire elements of the X-array probes using the formulae given in Bell and Mehta [14].

The hot-wire signals were digitized, along with the signals from the thermocouple, with the National Instruments AT-A2150 dynamic signal acquisition board. This board consists of 4 analog input channels, each of 16-bit resolution. Each of the analog input channels is preceded by a third-order Butterworth low-pass analog anti-aliasing filter with an 80 kHz cut off. The filtered signal is sampled with a 1-bit delta-sigma modulating analog sampler at 64 times the chosen sampling rate. This reduces the quantization noise considerably. The output of the sampler is then fed to a digital anti-aliasing filter, which is built into the A/D converter chip, and the output of this filter re-samples the signal to the data rate, namely, 16-bit digital samples. It should be noted that all 4 analog input channels can be sampled simultaneously and, therefore, sample-and-hold units, which are required for successive approximation and dual slope A/D converters, are not needed here. The input range of the AT-A2150 board is ± 2.828 volts (or 2 volts rms), so amplification was only needed for the thermocouple signal and not for the hot-wire signals. The hot-wire power-law relationship ($E^2 = A + BU_{\text{eff}}^n$) was linearized, in effect the U_{eff} signal from each of the hot-wire sensors was expressed as: $U_{\text{eff}} = ((E^2 - A)/B)^{(1/n)}$, in the data reduction software. The mean velocity and turbulence data were obtained from records containing 8192 samples obtained at a sampling rate of 4 kHz. The number of samples and the sampling rate, resulting in the sampling time, were chosen to minimize the data acquisition time, thus also minimizing hot-wire drift, and to ensure convergence of the mean velocities and the turbulence statistics. Tests of convergence of the measured quantities confirmed the values chosen.

The mean static pressure measurements were made with a 2.3 mm diameter pitot- tube, made of stainless steel with an ellipsoidal head and four circumferentially located static pressure holes, connected to a DATAMETRICS pressure transducer and an electronic manometer. These signals were also digitized with the AT-A2150 board but a voltage divider was needed to bring the signals into the input range of the board.

3. Initial conditions

The mean streamwise velocity at the centre of the sharp-edged orifice or the contoured nozzle exit plane was 61 m/s and this resulted in a Reynolds number, based on the orifice or nozzle diameter, $D_e = 45.3$ mm, of 1.84×10^5. The corresponding streamwise turbulence intensity at the same location on the exit plane was 0.4%. The mean streamwise velocity and streamwise turbulence intensity profiles close to the exit plane (at $X/D_e = 0.28$) are shown in Figs. 4 and 5, respectively. The mean streamwise velocity profile of the sharp-edged orifice jet is clearly saddle-backed while that of the contoured nozzle jet is essentially flat at this location. It is also observed that the profile for the contoured nozzle jet is wider than that of the sharp-edged orifice jet. This is due to the vena contracta effect which causes a narrowing of the sharp-edged orifice jet initially. The streamwise turbulence intensity profile is flat, at about 0.54%, in the central region, where the mean streamwise velocity is nearly constant. The streamwise turbulence intensities increase and reach their maximum values in the shear layer regions in both jets. Since the normalizing centerline mean streamwise velocity (U_{cl}) is much higher in the sharp-edged orifice jet, due to the vena contracta effect, it is clear that the absolute rms fluctuating velocities are much higher in the sharp-edged orifice jet compared to the contoured nozzle jet at this location.

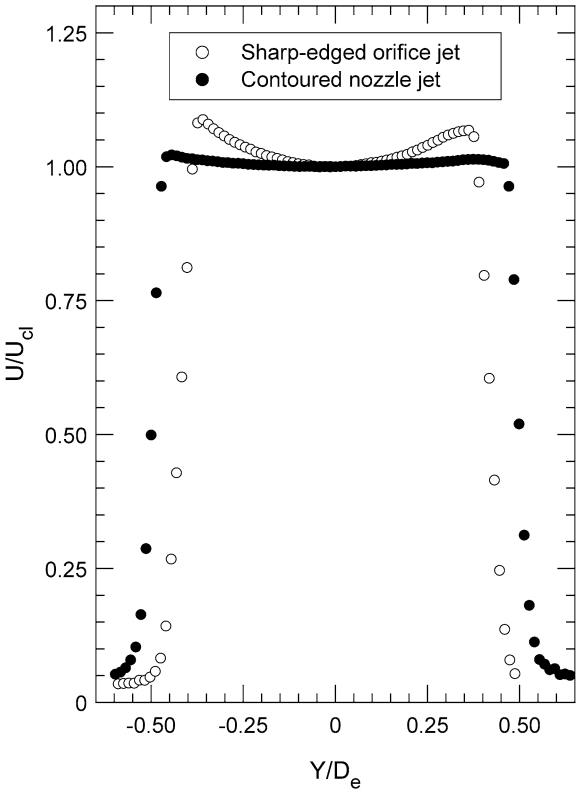

Fig. 4. Mean streamwise velocity profiles at $X/D_e = 0.28$.

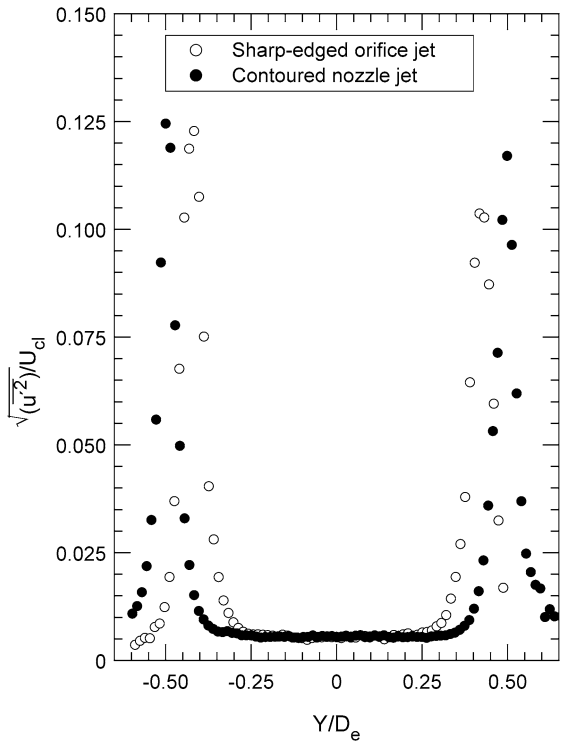

Fig. 5. Streamwise turbulence intensity profiles at $X/D_e = 0.28$.

4. Results and discussion

4.1. Mean streamwise velocity decay on the jet centerline

The decay of the mean streamwise velocity along the centreline of the jets is shown in Fig. 6. U_{cl} is the mean streamwise velocity anywhere on the jet centreline and U_{exit} is the mean streamwise velocity at the centre of the nozzle exit plane. In the case of the flow from the sharp-edged orifice, U_{exit} is the bulk-mean exit velocity. The vena contracta effect which results in the acceleration of the jet close to the exit plane, up to about $X/D_e = 0.25$, is clearly evident in the jet from the sharp-edged orifice but is absent in the other jet. The potential core region, characterized by constant velocity, is followed by a gradual decay of the mean streamwise velocity to asymptotic values, which are approximately the same in both jets, in the far flow field. The "potential core lengths", which should be understood in this context as the distances from the exit planes beyond which the centerline mean streamwise velocities decrease monotonically from approximately constant values, of the sharp-edged orifice and contoured nozzle jets are $3.50D_e$ and $4.26D_e$, respectively, and this implies higher mixing in the sharp-edged orifice jet compared to that in the contoured nozzle jet. The data shown in Fig. 6 are presented as an inverse decay plot in Fig. 7 to facilitate the process of obtaining the mean streamwise velocity decay rates of the jets. A flat initial region, representing the "potential core", is again clearly evident in both jets. However, while the flat region is at $U_{exit}/U_{cl} = 1$ in the case of the contoured nozzle round jet, U_{exit}/U_{cl} is less than one in the flat region in the sharp-edged orifice jet, due to the vena contracta effect. The data in the far field have been fitted by linear regression to:

$$\frac{U_{exit}}{U_{cl}} = K_u(X/D_e + C_u). \tag{4.1}$$

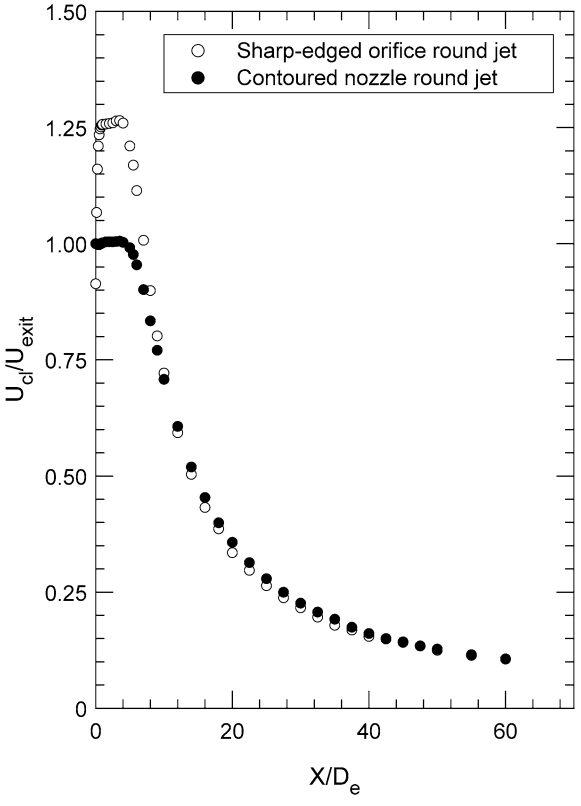

Fig. 6. Mean streamwise velocity decay along the jet centreline.

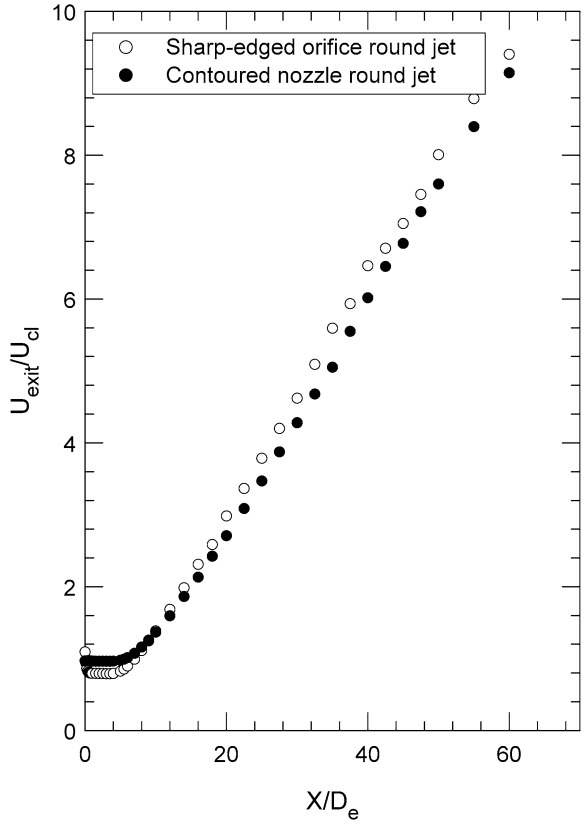

Fig. 7. Inverse mean streamwise velocity decay.

K_u is the mean streamwise velocity decay rate on the jet centreline and C_u is the kinematic virtual origin of the jet. In the region $18 \leqslant X/D_e \leqslant 55$, the data for the sharp-edged orifice jet and for the contoured nozzle jet can be described by:

$$\frac{U_{exit}}{U_{cl}} = 0.167(X/D_e - 2.15) \tag{4.2}$$

and

$$\frac{U_{exit}}{U_{cl}} = 0.164(X/D_e - 3.65), \tag{4.3}$$

respectively.

The values of K_u for the round jets of the present study and for the round jets investigated by others are shown in Table 1.

The fact that the K_u value for the sharp-edged orifice jet is larger than that of the contoured nozzle jet of the present study, albeit only slightly, implies higher mixing in the sharp-edged orifice jet compared to that in the contoured nozzle jet. This finding is in agreement with the results of Quinn and Militzer [10] and those of Mi et al. [11], who used the temperature field in their study. Differences in the K_u values may be, as is well known, due to the initial conditions in the different flow facilities, in particular, as has been shown by Malmstrom, Kirkpatrick, Christensen and Knappmiller [15], the exit plane Reynolds number. It is quite possible that normalizing X by the diameter of the jet at the vena contracta in Fig. 7, in the case of the sharp-edged orifice jet, may lead to K_u values which are the same in both jets but this was not explored in the present study.

Table 1
Mean streamwise velocity decay rates on the jet centreline for round jets

Investigators	Nozzle type	K_u	Range	Reynolds number
Present	Contoured	0.164	$18 \leqslant X/D_e \leqslant 55$	1.84×10^5
Present	Sharp-edged orifice	0.167	$18 \leqslant X/D_e \leqslant 55$	1.84×10^5
Wygnanski and Fiedler [1]	Contoured	0.169	$10 \leqslant X/D_e \leqslant 50$	8.64×10^4
Rodi [2]	Contoured	0.160	$50 \leqslant X/D_e \leqslant 75$	8.08×10^4
Panchapasekan and Lumley [3]	Contoured	0.165	$30 \leqslant X/D_e \leqslant 160$	1.1×10^4
Obot et al. [9]	Square-edged orifice	0.190	$X/D_e \geqslant 4$	1.3×10^4

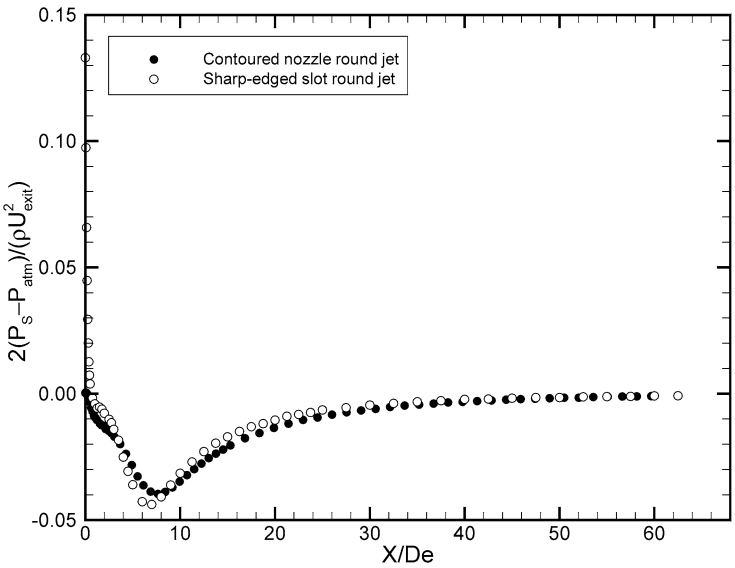

Fig. 8. Mean static pressure variation on the jet centreline.

4.2. Mean static pressure distribution on the jet centreline

The mean static pressure distribution on the jet centreline for both of the round jets of the present study is shown in Fig. 8. P_s is the mean static pressure, P_{atm} is the atmospheric pressure and ρ is the density of the jet fluid. In the very near flow field of the sharp-edged orifice round jet, the mean static pressure drops from a positive value (i.e., above atmospheric pressure) at the slot exit plane to zero (i.e., atmospheric pressure) as a result of the acceleration of the jet fluid brought about by the vena contracta effect. The further decrease in the mean static pressure to negative values is triggered by the rapid production of turbulence from mean flow shear in the near flow field. In the case of the contoured nozzle round jet, the mean static pressure is initially atmospheric and then decreases to negative values as turbulence is produced from mean flow shear. The speed with which the mean static pressure in a jet recovers from negative values to atmospheric pressure can perhaps be interpreted as a measure of the level of mixing that is taking place within the jet. Based upon this, mixing in the sharp-edged orifice jet, which reaches a maximum negative mean static pressure at $X/D_e = 7.0$ compared to $X/D_e = 7.7$ for the contoured nozzle jet, is higher than that which takes place in the jet issuing from the contoured nozzle.

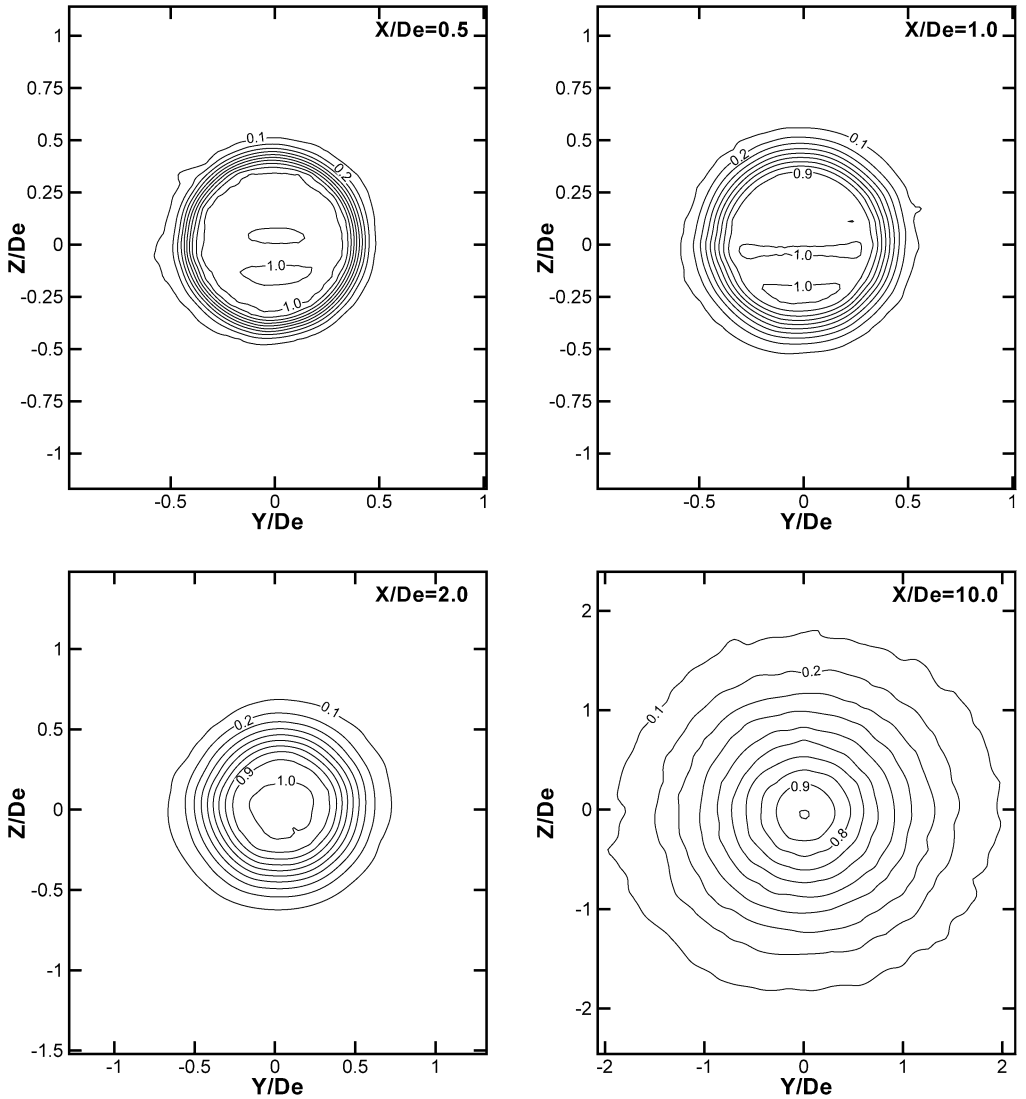

Fig. 9. (a) Mean streamwise velocity (U/U_{cl}) contour maps for the sharp-edged orifice jet. (b) Mean streamwise velocity (U/U_{cl}) for the contoured nozzle jet.

4.3. Mean streamwise velocity contour maps

Prior to presenting and discussing the mean streamwise velocity contour maps and the other results, it is perhaps necessary to recall that the contraction is circular at its upstream end and decreases in diameter until it becomes square at its downstream end. This square exit shape of the contraction will not affect the axisymmetry of the flow from the sharp-edged orifice since this flow is separated both upstream and downstream of the orifice exit plane. The flow from the smooth contracting nozzle, which has no upstream separation, will be influenced, at least in the near flow field considered here by the square shape of the contraction exit plane.

The contour maps for the mean streamwise velocity field of the two test jets are shown in Fig. 9. U has been normalized by U_{cl} in each of the contour maps. Initially, at $X/D_e = 0.5$, the contours in both jets have the round shape imposed by the slot or nozzle exit and they are very closely spaced, indicating that very little mixing has taken place at this location. At $X/D_e = 1.0$, the contours are still round, as is to be expected, and the spacing between the contour levels has increased. Further downstream, at $X/D_e = 2.0$, the contours in the sharp-edged jet are really round (Fig. 7(a)) but those in the contoured nozzle jet are distinctly different from the round shape (Fig. 7(b)). This

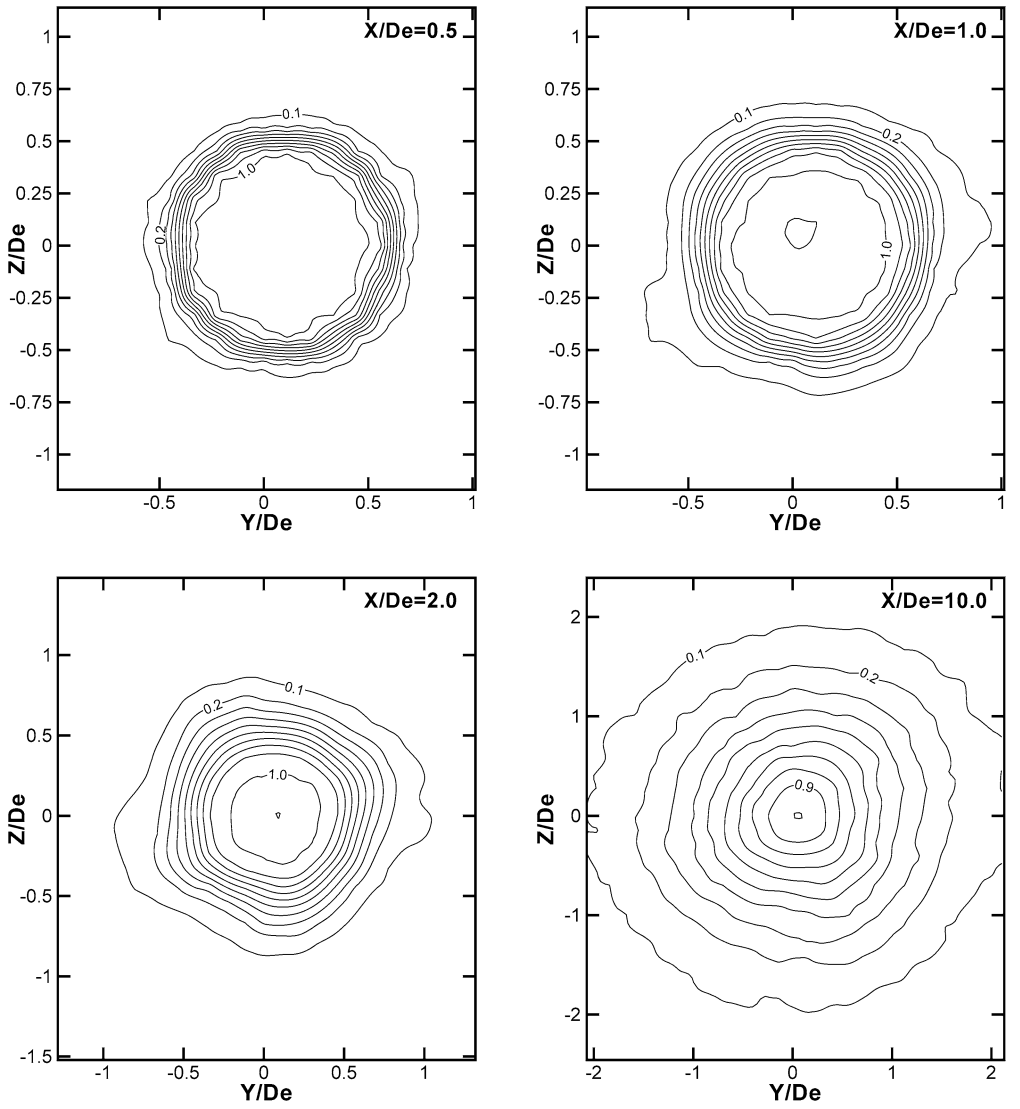

Fig. 9 (*continued*).

difference from the round shape of the mean velocity contour maps contoured nozzle flow is brought about by the square exit shape of the contraction as mentioned previously. The contoured nozzle jet flow, in spite of the square shape of the mean streamwise velocity contours at $X/D_e = 2.0$, should not be confused with the flow of a jet from a square slot in which, as has been shown by Quinn [16], the mean streamwise velocity contours continuously change shape downstream due to curvature-based vortex induction until an axisymmetric shape is attained. The difference in the shape of the mean streamwise velocity contour maps in the two jets observed at $X/D_e = 2.0$ is still evident at $X/D_e = 10.0$. The results of the contoured nozzle jet flow are consistent with those of previous studies of this flow configuration, as the comparisons made in sections 4.1, 4.4, 4.5 and 4.10 of this article have shown and will show. The effect of the upstream square bias on the development of the contoured nozzle flow, therefore, seems negligible but future studies should avoid such a bias whenever possible.

4.4. Jet half-velocity widths

The development of the jet half-velocity widths is shown in Fig. 10 for the two round jets studied here. The half-velocity width of a jet is defined as the distance from the centerline of the jet to the point where the mean streamwise velocity is half its value on the jet centerline. $B_{1/2}$ is the jet half-velocity width. The jet half-velocity widths in both jets have a more or less flat initial region which is followed by a region in which the jet half-velocity widths increase in a linear fashion. The jet half-velocity widths in the contoured nozzle round jet are slightly larger than those in the sharp-edged slot round jet in the initial region. This may be due to the vena contracta effect which causes the sharp-edged round jet to contract initially. The data in the aforementioned linear region have been fitted by linear regression to:

$$\frac{B_{1/2}}{D_e} = K_s(X/D_e + C_s). \tag{4.4}$$

K_s is the spreading rate and C_s is the geometric virtual origin. The K_s values obtained by previous investigators of round jets and those from the present study are shown in Table 2.

The K_s value for the sharp-edged orifice jet is larger than that of the contoured nozzle jet of the present study implying higher mixing in the sharp-edged orifice jet compared to that in the contoured nozzle jet. This finding is in agreement with results of Quinn and Militzer [10] and those of Mi et al. [9], who examined the temperature half-widths in their study. It is interesting to note that the spreading rate of the present contoured nozzle round jet agrees exactly with that of Panchapasekan and Lumley [3], who used a flying hot-wire in their study. Differences in the K_s values may be, as is well known, due to the initial conditions in the different flow facilities.

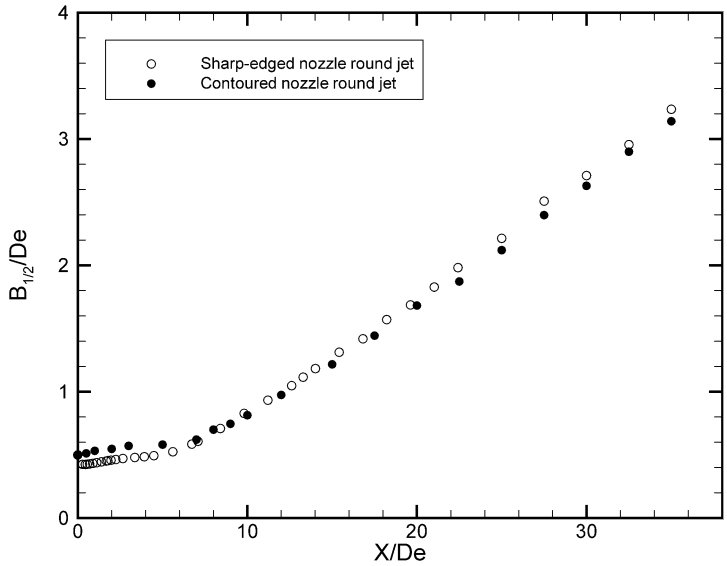

Fig. 10. Development of the jet half-velocity widths.

Table 2
Spreading rates for round jets

Investigators	Nozzle type	K_s	Range	Reynolds number
Present	Contoured	0.096	$15 \leqslant X/D_e \leqslant 31$	1.84×10^5
Present	Sharp-edged orifice	0.098	$15 \leqslant X/D_e \leqslant 31$	1.84×10^5
Wygnanski and Fiedler [1]	Contoured	0.086	$10 \leqslant X/D_e \leqslant 50$	8.64×10^4
Rodi [2]	Contoured	0.086	$50 \leqslant X/D_e \leqslant 75$	8.08×10^4
Panchapasekan and Lumley [3]	Contoured	0.096	$30 \leqslant X/D_e \leqslant 160$	1.1×10^4
Obot et al. [9]	Square-edged orifice	0.088	$X/D_e \geqslant 4$	1.3×10^4

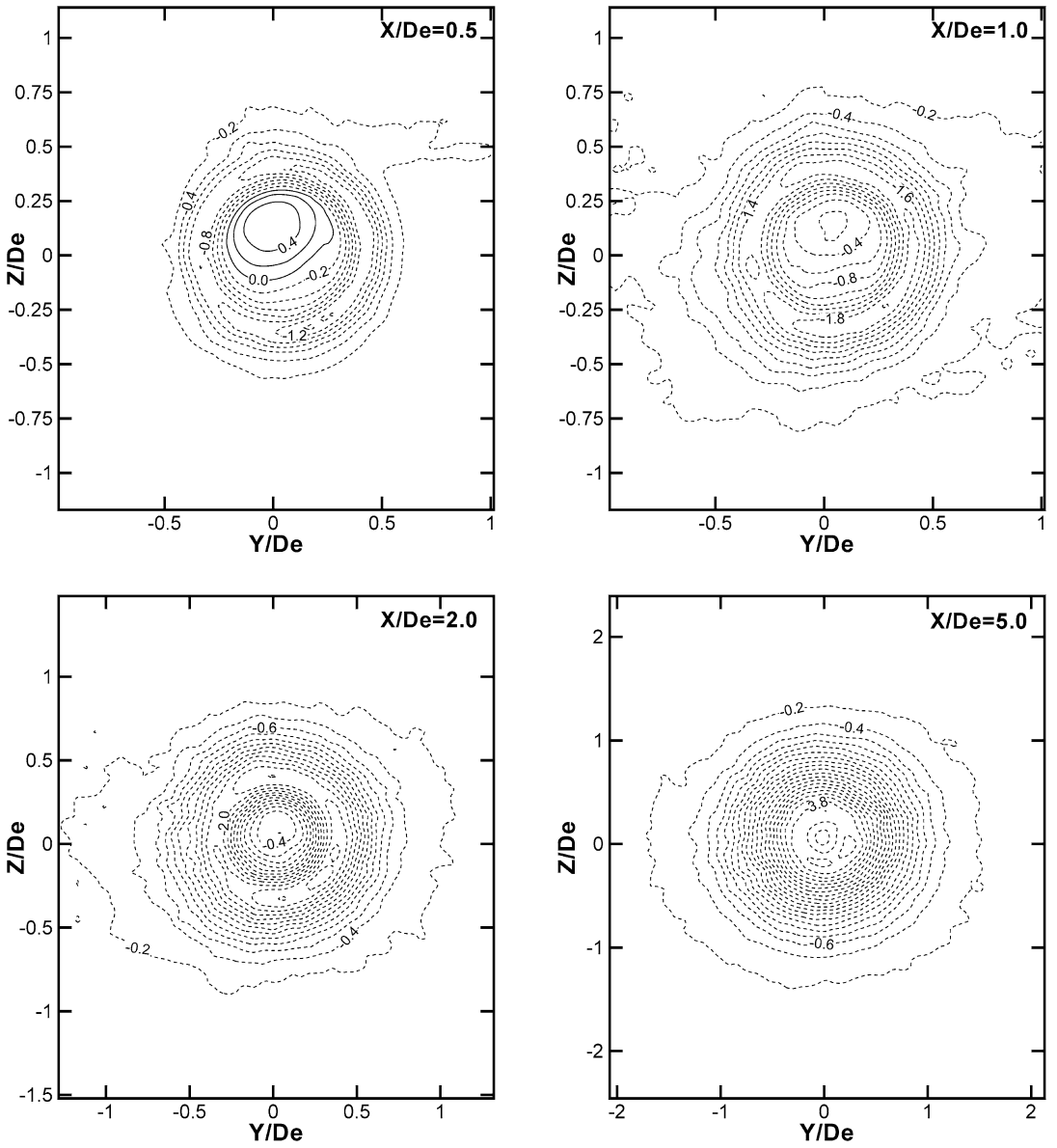

Fig. 11. (a) Mean static pressure $(2(P_s - P_{atm})/(\rho U_{cl}^2) \times 100)$ contour maps for the sharp-edged orifice jet. (b) Mean static pressure $(2(P_s - P_{atm})/(\rho U_{cl}^2) \times 100)$ contour maps for the contoured nozzle jet.

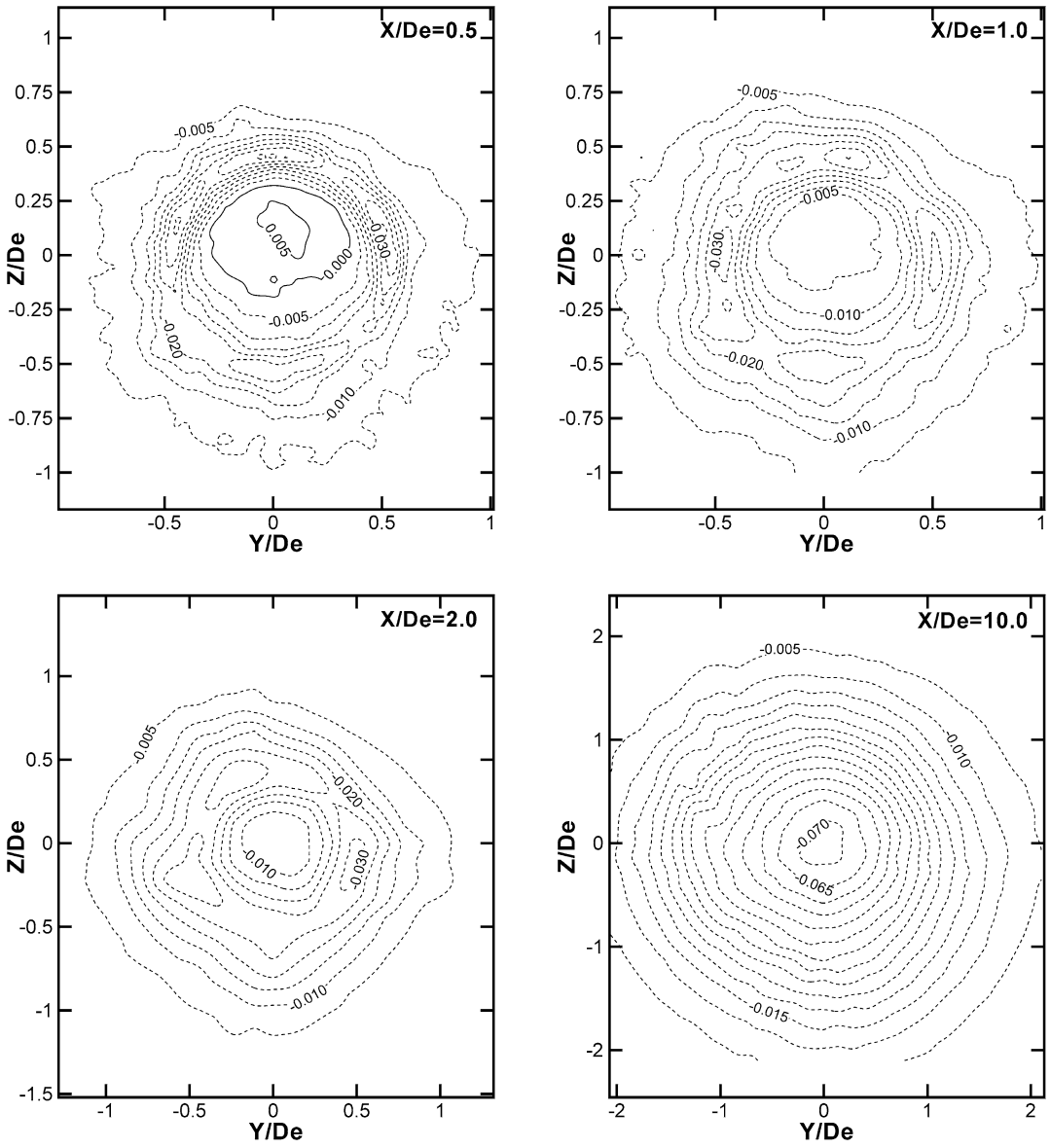

Fig. 11 (*continued*).

4.5. Mean static pressure contour maps

The mean static pressure contour maps for the two jets are shown in Fig. 11. In each contour map, the normalized mean static pressure $((2(P_s - P_{atm}))/(\rho U_{cl}^2))$ has been amplified by a factor of 100. The mean static pressure distribution along the jet centreline presented in Fig. 8 showed positive values up to about $X/D_e = 1$ and negative values up to about $X/D_e = 20$ in the sharp-edged orifice round jet. It is, therefore, not surprising to find positive mean static pressures in the central region of the sharp-edged orifice round jet at $X/D_e = 0.5$ and negative mean static pressures throughout the jet at the other three locations shown in Fig. 11(a). It is clear that the flow of ambient fluid will generally be induced into the jet as a result of the difference in pressure between the ambient and the jet. This is the case beyond $X/D_e = 0.5$ in the sharp-edged orifice round jet (Fig. 11(a)) and at all four locations in the contoured nozzle round jet (Fig. 11(b)). At $X/D_e = 0.5$ in the sharp-edged orifice round jet (Fig. 11(a)), the small central region of positive mean static pressure within the jet will induce the flow of jet fluid to regions of negative mean static pressure.

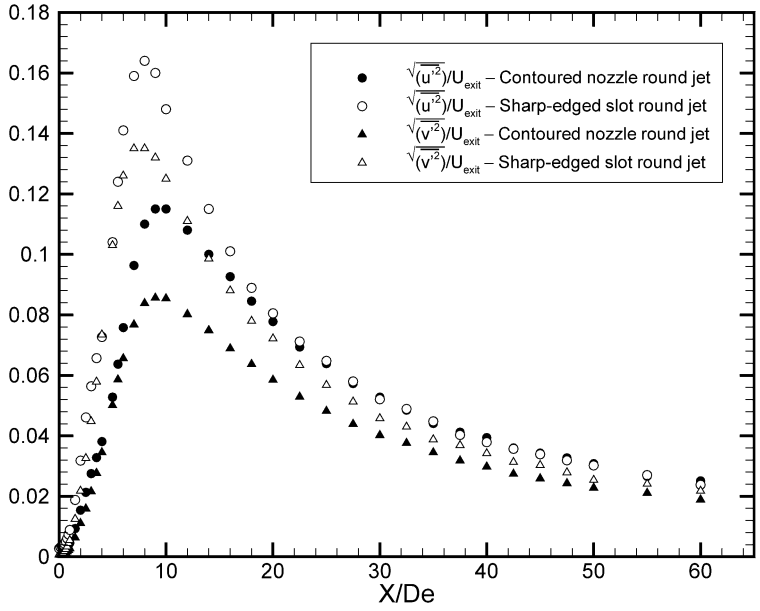

Fig. 12. Evolution of the turbulence intensities along the jet centreline.

4.6. Centreline turbulence intensities

The evolution of the streamwise ($\sqrt{\overline{u'^2}}/U_{\text{exit}}$) and spanwise ($\sqrt{\overline{v'^2}}/U_{\text{exit}}$) turbulence intensities along the jet centreline of the two jets is shown in Fig. 12. A steep initial increase in all the turbulence intensities, brought about by production due to mean flow shear in the shear layers and transport by diffusion to the jet centreline, is observed. The turbulence intensities in the sharp-edged orifice jet peak (at $X/D_{\text{e}} = 8.0$) before the turbulence intensities in the contoured nozzle jet, which are generally lower, reach their peak values (at $X/D_{\text{e}} = 9.0$), an indication of higher mixing in the sharp-edged orifice jet. It should be recalled that the mean static pressure along the jet centreline in the sharp-edged orifice jet, shown in Fig. 8, also starts to recover from negative values towards atmospheric pressure before the mean static pressure in the contoured nozzle jet does.

At $X/D_{\text{e}} = 60$ in the contoured nozzle flow, $\sqrt{\overline{u'^2}}/U_{\text{exit}} = 0.024$ and $\sqrt{\overline{v'^2}}/U_{\text{exit}} = 0.018$. These values compare very well to $\sqrt{\overline{u'^2}}/U_{\text{exit}} = 0.0235$ and $\sqrt{\overline{v'^2}}/U_{\text{exit}} = 0.0183$ found at the same location in the contoured nozzle jet studied by Panchapakesan and Lumley [3].

4.7. Streamwise Reynolds normal stress contour maps

Contour maps for the streamwise Reynolds normal stress ($\overline{u'^2}$) in the two jets are shown in Fig. 13. The normalized normal stress ($\overline{u'^2}/U_{\text{cl}}^2$) is amplified by a factor of 100 in each of the contour maps. The shapes of these contour maps correspond very closely to those of the mean streamwise velocity shown in Fig. 9 at the corresponding streamwise locations. Large or small values of the streamwise Reynolds normal stress are found, as is to be expected, in regions where the local shear in the mean streamwise velocity ($\partial U/\partial Y$) is large or small. In the production of the streamwise Reynolds normal stress, the major contribution is made by $-\overline{u'v'}\partial U/\partial Y$. This is why, as will become evident later, there is a close relationship between the streamwise Reynolds normal stress contour maps shown in Fig. 13 and the mean streamwise velocity contour maps shown in Fig. 9. Note that the deviation from the circular shape at $X/D_{\text{e}} = 2.0$, observed in the mean streamwise velocity contour map, is evident in the streamwise Reynolds normal stress contour map of the contoured nozzle round jet flow, an effect of the square exit shape of the contraction to which the contoured nozzle is attached as mentioned previously. The reader is reminded that the streamwise turbulence intensities along the jet centerline, shown in Fig. 12, were consistently higher in the sharp-edged orifice jet flow. This is important to note because the normalizing mean streamwise velocity (U_{exit}) in Fig. 12 is the same in both flows

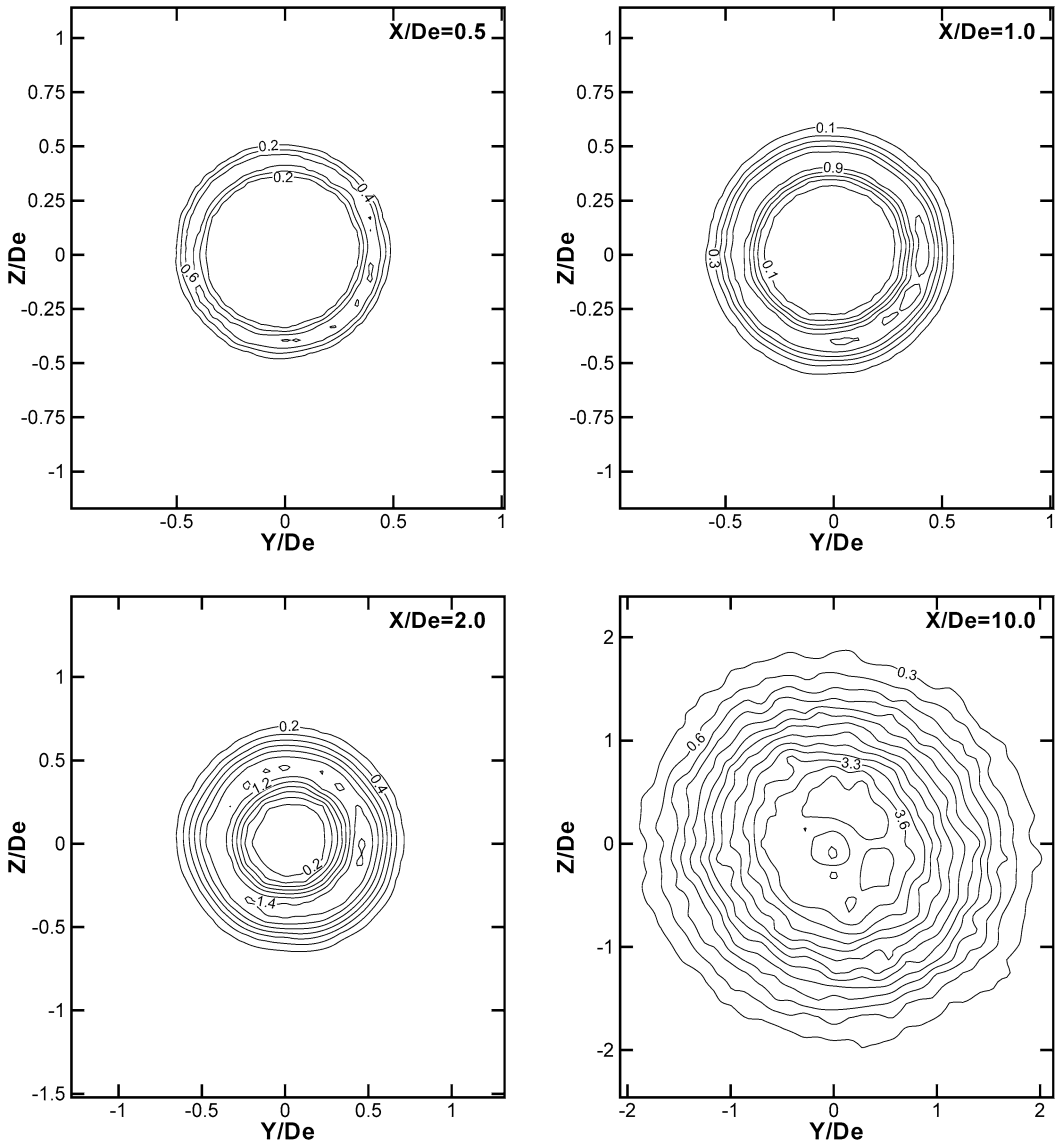

Fig. 13. (a) Streamwise Reynolds normal stress ($(\overline{u'^2})/(U_{\mathrm{cl}}^2) \times 100$) contour maps for the sharp-edged orifice jet. (b) Streamwise Reynolds normal stress ($(\overline{u'^2})/(U_{\mathrm{cl}}^2) \times 100$) contour maps for the contoured nozzle jet.

whereas the normalizing mean streamwise velocity (U_{cl}) in Fig. 13 varies from location to location and is generally higher in the sharp-edged orifice jet flow in the region of interest here as Fig. 6 shows. It should then be clear that the streamwise Reynolds normal stresses in the sharp-edged orifice jet are higher than those in the contoured nozzle jet, again indicating higher mixing in the sharp-edged orifice jet flow.

4.8. Spanwise Reynolds primary shear stress contour maps

The spanwise Reynolds primary shear stress ($-\overline{u'v'}$), which represents the mean rate of transfer of the spanwise component of the linear momentum through a unit area normal to the streamwise direction, contour maps are shown in Fig. 14. The normalized spanwise Reynolds primary shear stress ($\overline{-u'v'}/U_{\mathrm{cl}}^2$) contour maps have been amplified by a factor of 100 at each location. Contour maps for the local spanwise shear ($\partial U/\partial Y$) in the mean streamwise velocity are shown in Fig. 15 for the sharp-edged orifice jet to facilitate the discussion of the spanwise Reynolds

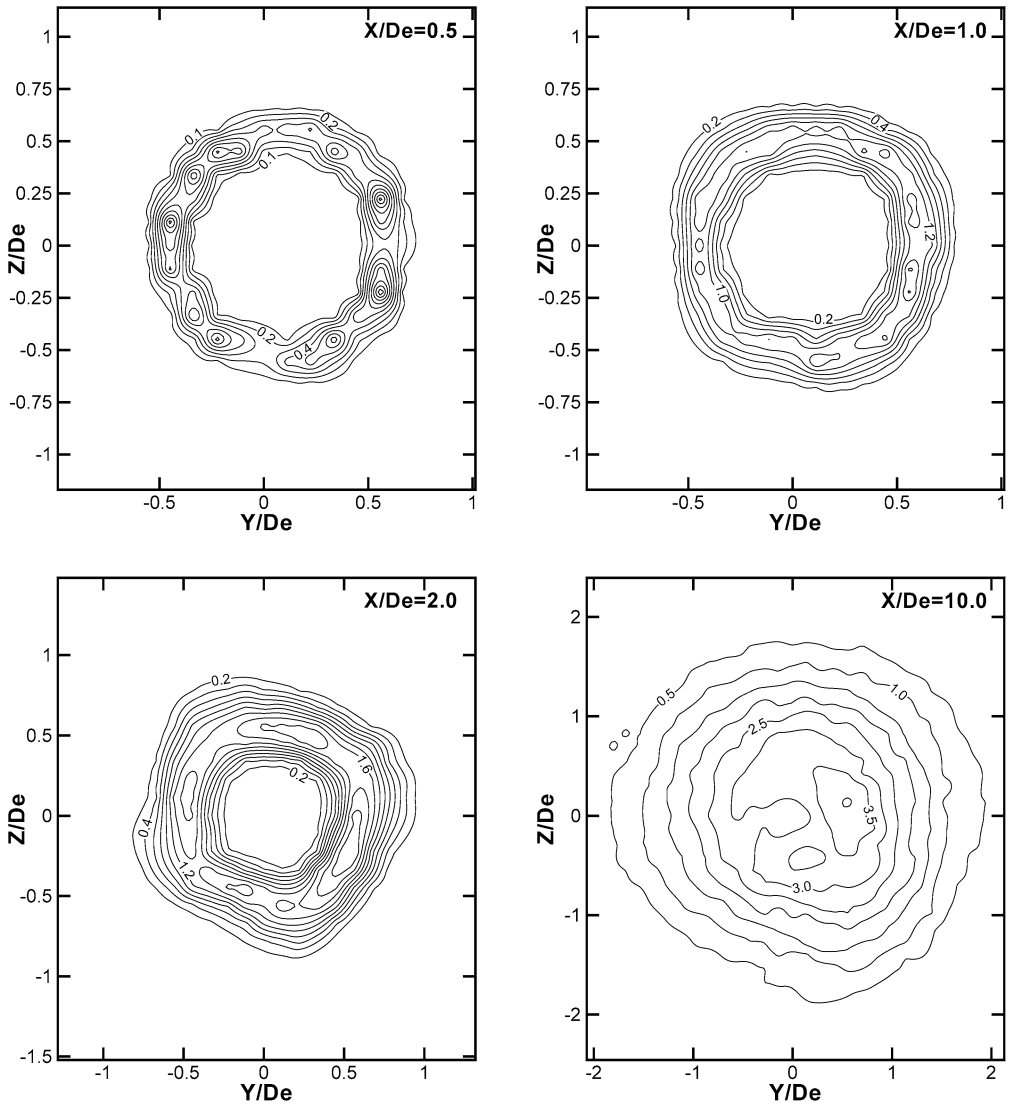

Fig. 13 (*continued*).

primary shear stress results. It is clear from Figs. 14(a) and 15 that the spanwise Reynolds primary shear stress is well correlated with the spanwise local shear in the mean streamwise velocity in the sharp-edged orifice jet flow. This is not surprising since the dominant term in the generation of $\overline{u'v'}$ by the mean flow is: $\overline{v'^2}\partial U/\partial Y$, where $\overline{v'^2}$ is the spanwise Reynolds normal stress. This close correspondence between $\overline{u'v'}$ and $\partial U/\partial Y$ suggests that the stress-strain relationship: $-\overline{u'v'} = \nu_t \partial U/\partial Y$ is valid at least in the sharp-edged orifice round jet flow, implying that an isotropic turbulence model, such as the k–ε model, can be used to close the set of governing equations in the numerical computation of the sharp-edged orifice jet flow. ν_t is the kinematic eddy viscosity, k is the turbulence kinetic energy and ε is the dissipation rate of turbulence kinetic energy. The behavior of the spanwise Reynolds primary shear stress in the contoured nozzle jet flow is similar to that, just described, observed in the sharp-edged orifice jet flow. However, the spanwise Reynolds primary shear stresses in the contoured nozzle jet flow generally have smaller values than those found in the sharp-edged orifice jet flow when one considers that U_{cl}, the normalizing mean streamwise velocity, has higher values in the sharp-edged orifice jet flow at each of the locations shown in Fig. 14 as was mentioned previously. Momentum transfer by the spanwise Reynolds primary shear stresses (i.e., mixing) is, consequently, higher in the sharp-edged orifice jet flow.

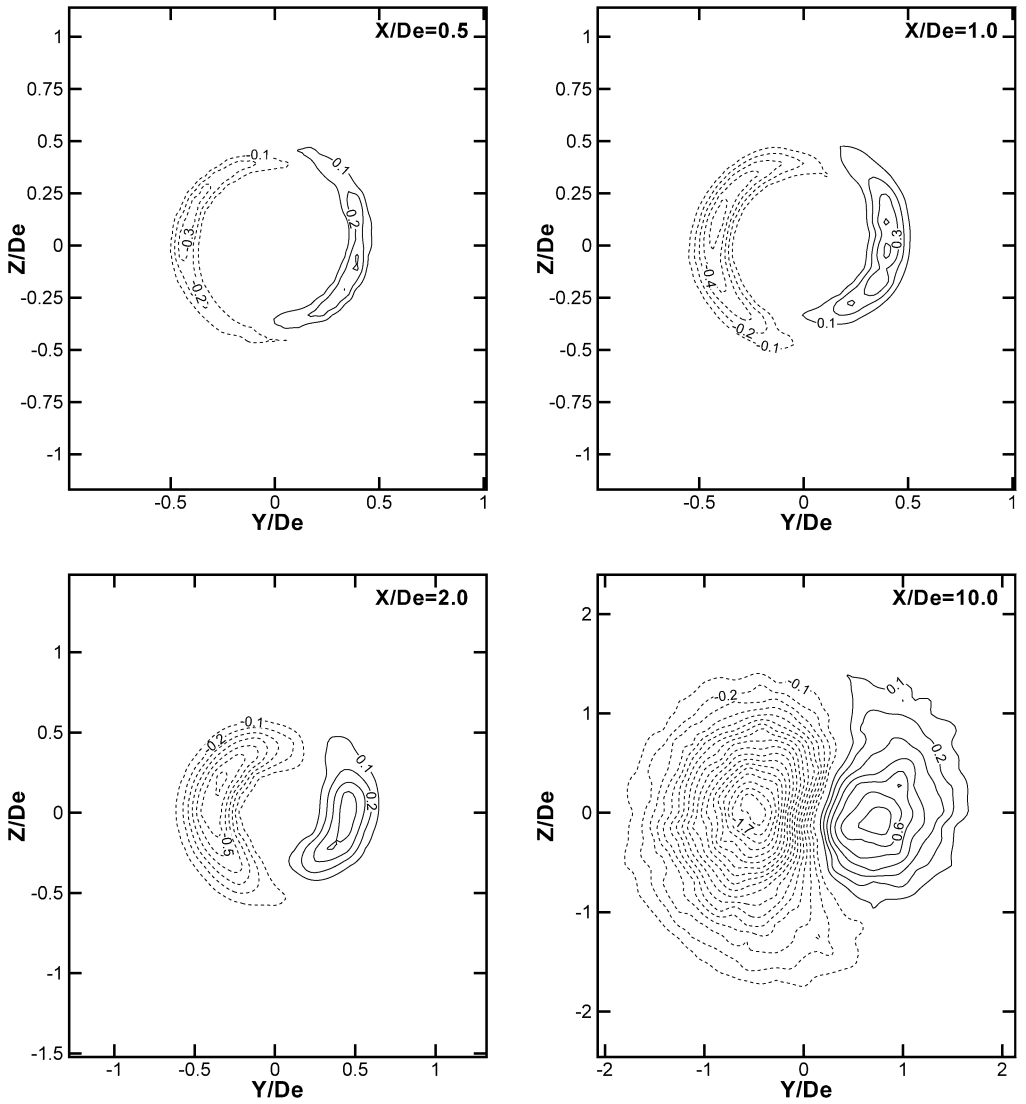

Fig. 14. (a) Spanwise Reynolds primary shear stress $((\overline{u'v'})/(U_{cl}^2) \times 100)$ contour maps for the sharp-edged orifice jet. (b) Spanwise Reynolds primary shear stress $((\overline{u'v'})/(U_{cl}^2) \times 100)$ contour maps for the contoured nozzle jet.

4.9. Distribution of the autocorrelation coefficients of the fluctuating streamwise velocity on the jet centerline

The distribution of the autocorrelation coefficients ($\rho(\tau)$) of the fluctuating streamwise velocity (u') at various locations on the jet centreline in the near field of the two jets is shown in Fig. 16. τ is the time delay. As it is well known, the autocorrelation and power spectrum have an inverse spreading relationship since both of these functions are Fourier Transform pairs. As a result, if the power spectrum is very narrow, the autocorrelation coefficient distribution will oscillate with decreasing amplitude and with a frequency (here, 645.2 Hz as shown in Fig. 17(a)) equal to that at which the peak in the power spectrum is centered, as can be seen at $X/D_e = 0.5$, 1.0 and 2.0 in Fig. 16(a) for the sharp-edged orifice jet. Such an autocorrelation coefficient distribution implies that the u' signal has a coherent component, characterizing the existence of large-scale coherent structures in the flow. In the case of the contoured nozzle jet, the distribution of the autocorrelation coefficients, shown in Fig. 16(b) at each of the three aforementioned streamwise locations, but especially so at $X/D_e = 2.0$, exhibits a long tail. Such a distribution of autocorrelation coefficients with a long tail has been observed before (see Cervantes de Gortari and Goldschmidt [17]) in a turbulent plane jet with a uniform exit plane mean streamwise velocity profile and it was thought to be the result of the "flapping" of the jet,

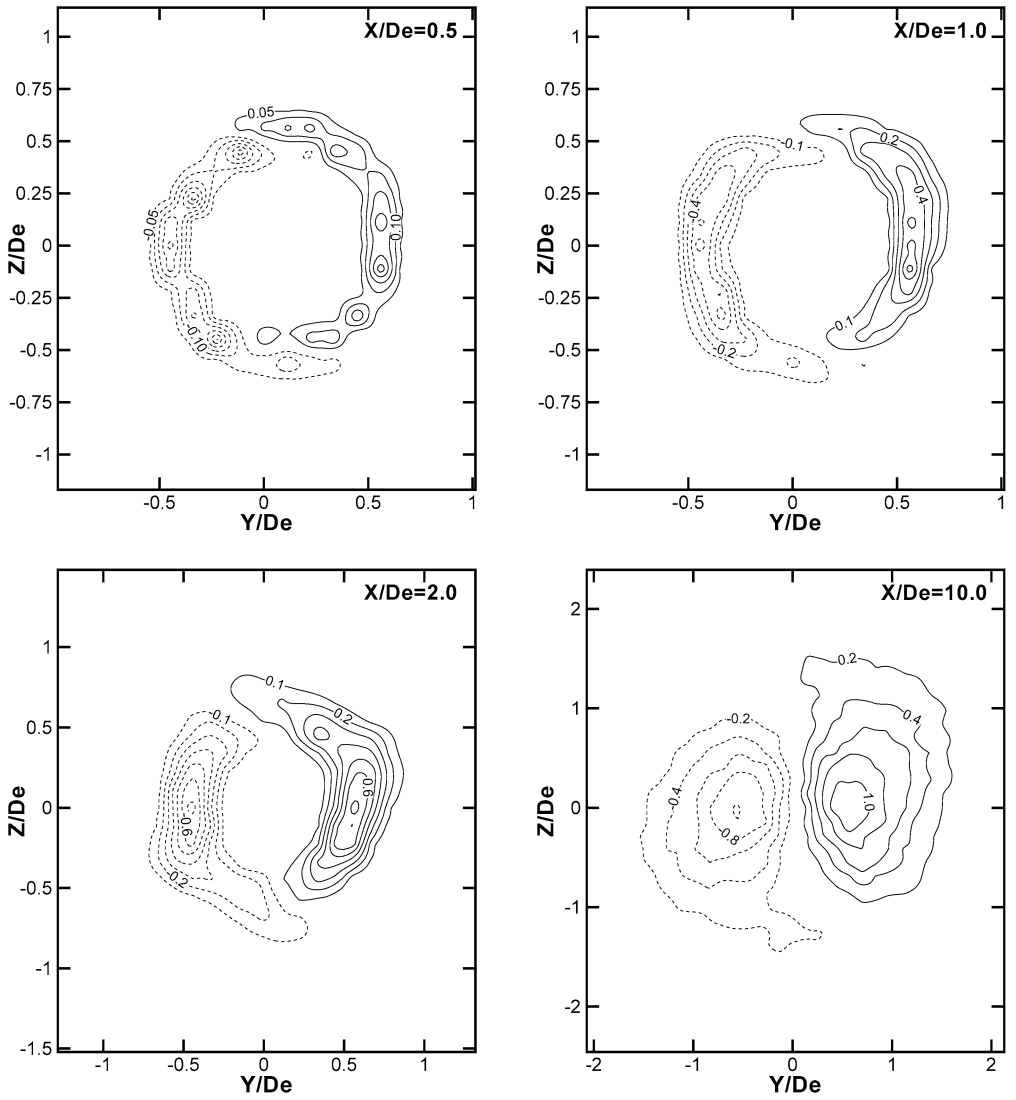

Fig. 14 (*continued*).

brought about by jet shear layer large-scale structures which cross the jet centreline. It appears, therefore, that the difference between the distribution of the autocorrelation coefficients of the streamwise fluctuating velocity in the two jets of the present study can be traced back to the exit plane mean streamwise velocity profiles, namely, uniform in the contoured nozzle jet and non-uniform in the sharp-edged orifice jet. The distribution of the autocorrelation coefficients at $X/D_e = 10.0$ represents that of a broadband signal which is characteristic of fully turbulent flow.

4.10. One-dimensional energy spectra of the streamwise fluctuating velocity on the jet centerline

The one-dimensional energy spectra of the fluctuating streamwise velocity on the centreline in the near flow field of the two jets are shown in Fig. 17. The one-dimensional energy spectra were obtained from Fast Fourier Transforms (FFT) of the digital hot-wire time-series data. At each location, the one-dimensional energy spectra ($\phi(f)$) have been normalized by the mean square of the streamwise velocity fluctuation ($\overline{u'^2}$). The logarithmic ordinate and linear abscissa scales are used in each of the plots in Fig. 17. The one-dimensional energy spectra exhibit, consistent with the distribution of the autocorrelation coefficients shown in Fig. 16, dominant peaks at a frequency, f, of 645.2 Hz at all the locations shown in both jet flows except at $X/D_e = 0.5$ in the contoured nozzle jet flow. The dominant peak

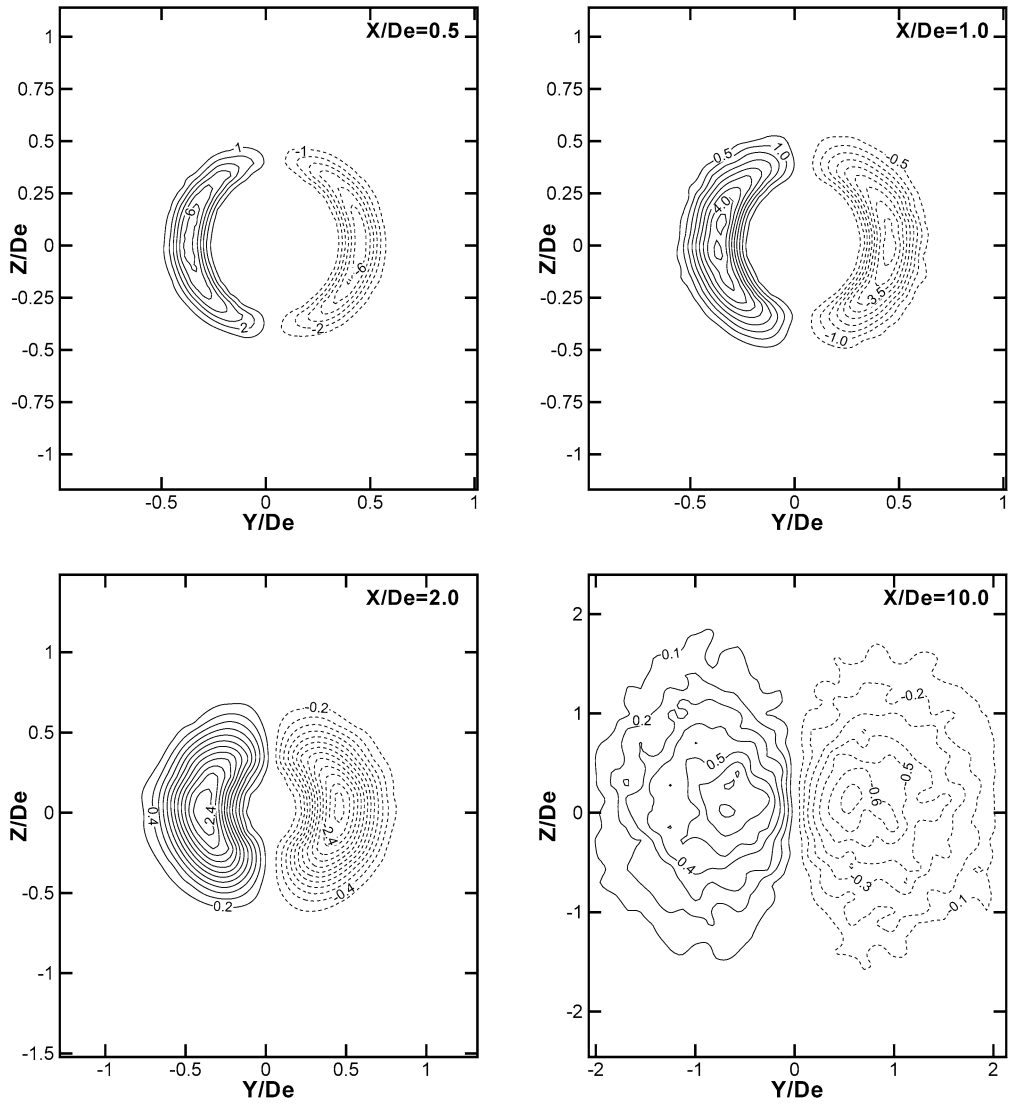

Fig. 15. Spanwise shear ($\partial U/\partial Y$) in the sharp-edged orifice jet mean streamwise velocity contour maps.

in the one-dimensional energy spectrum at this location is at a frequency of 277.7 Hz. The frequency corresponding to the dominant spectral peak at $X/D_e = 1.0$ and 2.0 results in a Strouhal number, defined here as $St_D = f D_e/U_{exit}$, of 0.46 for the contoured nozzle jet flow. It should be recalled that the "potential core" length of the contoured nozzle jet flow is $4.26D_e$, so the two streamwise locations: $X/D_e = 1.0$ and 2.0 are both within the potential core of the contoured nozzle jet flow. The Strouhal numbers found by some previous investigators of contoured nozzle jet flows are given in Table 3.

It should be noted that all the jet flows given in Table 3 were unforced or natural jet flows. Table 3 shows that the Strouhal number of the present contoured nozzle jet flow falls within the range of those found by previous investigators. Gutmark and Ho [21] attribute differences in Strouhal numbers of various jets to spatially coherent disturbances in the facilities used to generate the jets. A few more comments on the Strouhal numbers given in Table 3 are in order here. First, the $St_D = 0.44$ for the unforced round jet investigated by Crow and Champagne [18] is different from the 0.3 value for the excited jet studied by the same authors (see Fig. 30, page 582 of Crow and Champagne [18]). The dominant peak in the spectrum is at a frequency of 272 Hz for the unforced jet while this peak is at a frequency of 185 Hz for the excited jet. It should, in addition, be noted that the nozzle diameter and exit mean streamwise velocity were 0.0508 m and 31.4 m/s, respectively. Second, while all the other data in Table 3 were acquired on the jet centre-

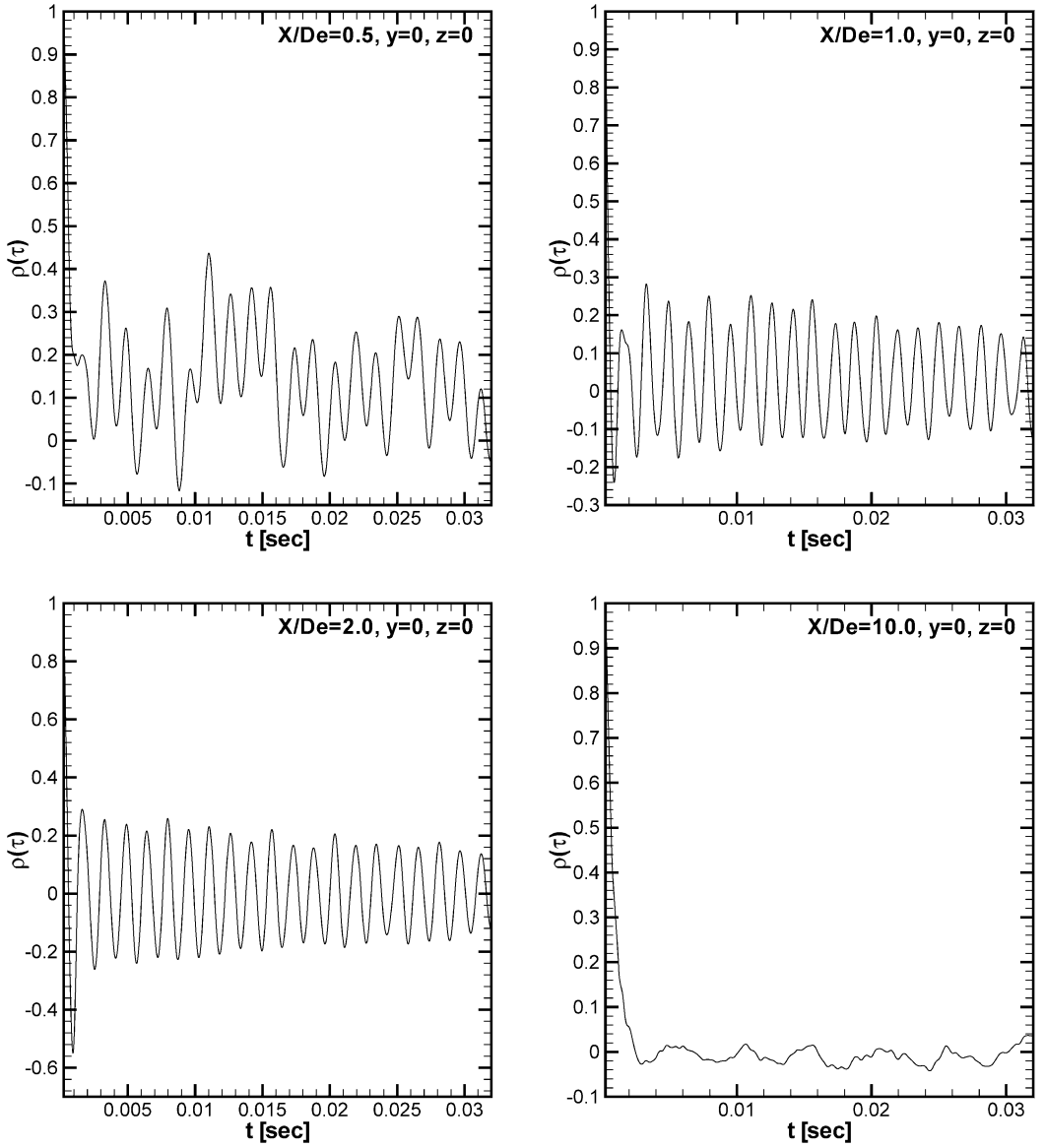

Fig. 16. (a) Distribution of the autocorrelation coefficients of the fluctuating streamwise velocity on the centerline of the sharp-edged orifice jet. (b) Distribution of the autocorrelation coefficients of the fluctuating streamwise velocity on the centerline of the contoured nozzle jet.

Table 3
Strouhal numbers for contoured nozzle round jet flows

Investigator	Exit plane Reynolds number based on the nozzle diameter	Strouhal number based on the nozzle diameter	Streamwise location (X/D_e)
Crow and Champagne [18]	1.06×10^5	0.44	4
Ko and Davies [19]	1.25×10^5, 2.5×10^5	0.43	3
Yule [20]	4.5×10^3	0.5	3
	7.1×10^3	0.29	4
	2.1×10^4	0.33	4
	2×10^5	0.43	4
Mi et al. [11]	1.6×10^4	0.4	3

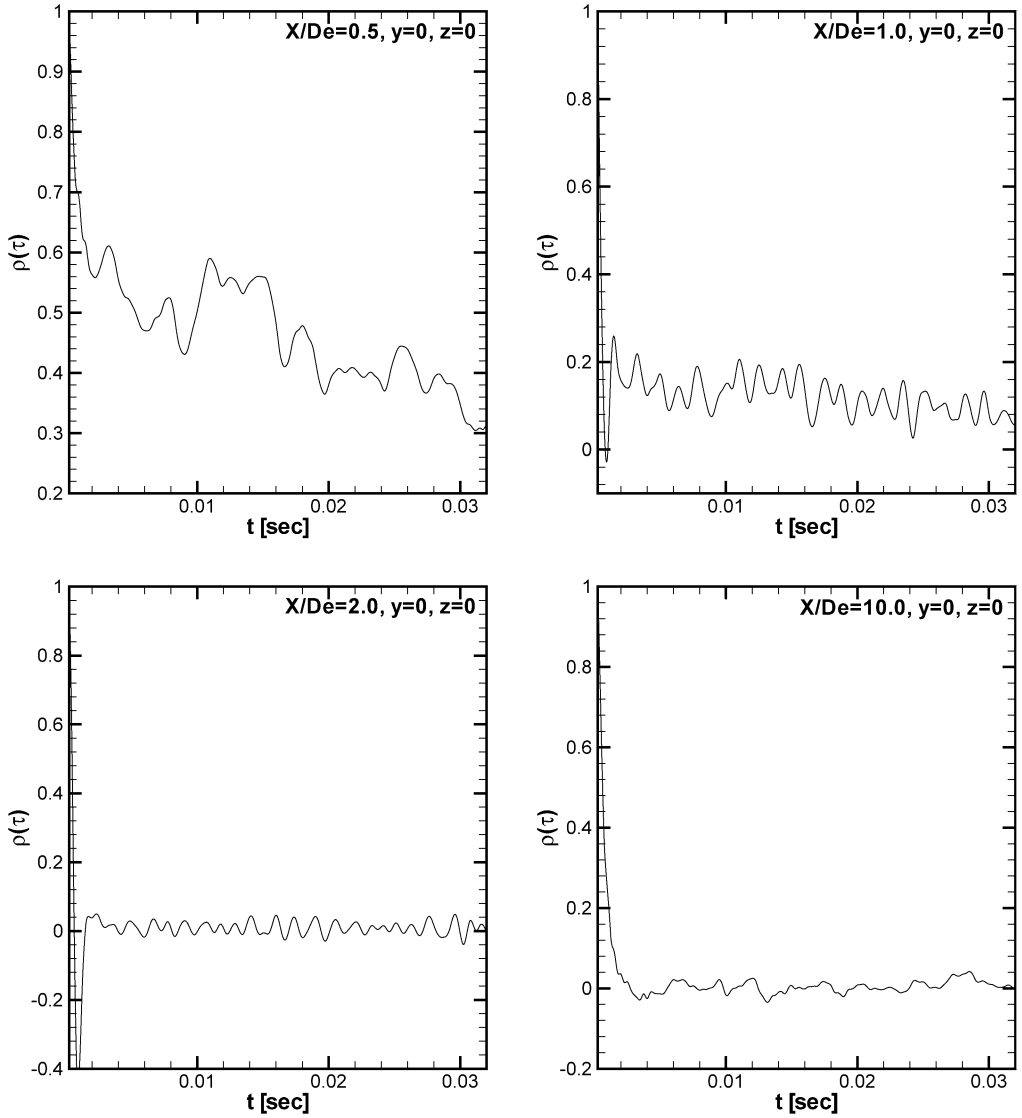

Fig. 16 (*continued*).

line, those of Mi et al. [11] and Yule [20] were obtained in the shear layer. It is known (see, e.g., Hussain [22]) that the frequency corresponding to the dominant peak in the spectrum varies not only in the streamwise direction but also, and considerably so, in the spanwise direction (i.e., in the shear layer).

The Strouhal number on the jet centreline at $X/D_e = 1.0$, 2.0 and 3.50 (the end of the "potential core" region) in the sharp-edged orifice jet is 0.45 while that measured in the shear layer at $X/D_e = 3.0$ in the orifice jet in the study of Mi et al. [11] is 0.7. The difference in the measurement location in the two studies may, as noted previously, account for the difference in the two values of the Strouhal number.

The magnitudes of the spectral peaks are very much higher in the sharp-edged orifice jet (Fig. 17(a)), especially when one considers the fact that the $\overline{u'^2}$ values, which are used to normalize the one-dimensional spectra ($\phi(f)$), are higher in the jet from the sharp-edged orifice than in the jet from the contoured nozzle (Fig. 17(b)). This implies higher energy content of the spectra at the preferred mode in the sharp-edged orifice jet. The peaks in the one-dimensional energy spectra indicate, like the decaying periodic distribution of the autocorrelation coefficients on the jet centerline, the passage of large-scale coherent structures. The one-dimensional energy spectrum of the fluctuating streamwise velocity at $X/D_e = 10.0$ is in both jets broadband, a characteristic of fully turbulent flow.

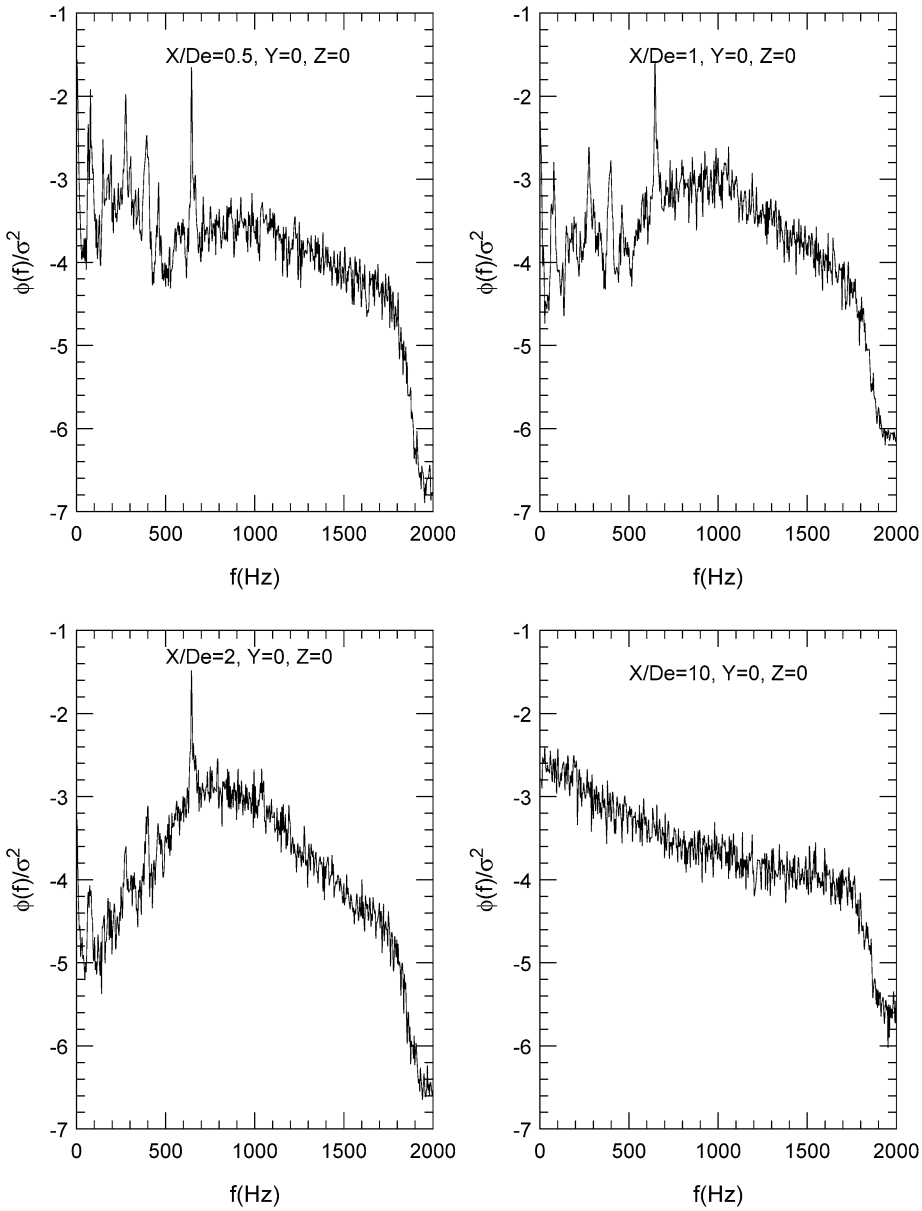

Fig. 17. (a) One-dimensional spectra of the fluctuating streamwise velocity on the centreline of the sharp-edged orifice jet. (b) One-dimensional spectra of the fluctuating streamwise velocity on the centreline of the contoured nozzle jet.

5. Conclusions

The near flow fields of isothermal, incompressible round turbulent free jets of air issuing from a sharp-edged orifice and from a contoured nozzle into still air surroundings have been studied experimentally using hot-wire anemometry and a pitot-static tube to determine the effects of upstream nozzle shaping on the evolution of the jets. The results obtained for the "potential core lengths", the mean streamwise velocity decay rates, the jet spreading rates, the mean static pressure recovery and the Reynolds normal and shear stresses show that mixing, which governs the evolution of the jet, is higher in the sharp-edged orifice jet than in the contoured nozzle jet. The results for the distribution of the autocorrelation coefficients of the streamwise fluctuating velocity show a marked difference in the evolution of the two jets, one of which has a uniform, and the other a non-uniform, exit plane mean streamwise velocity profile.

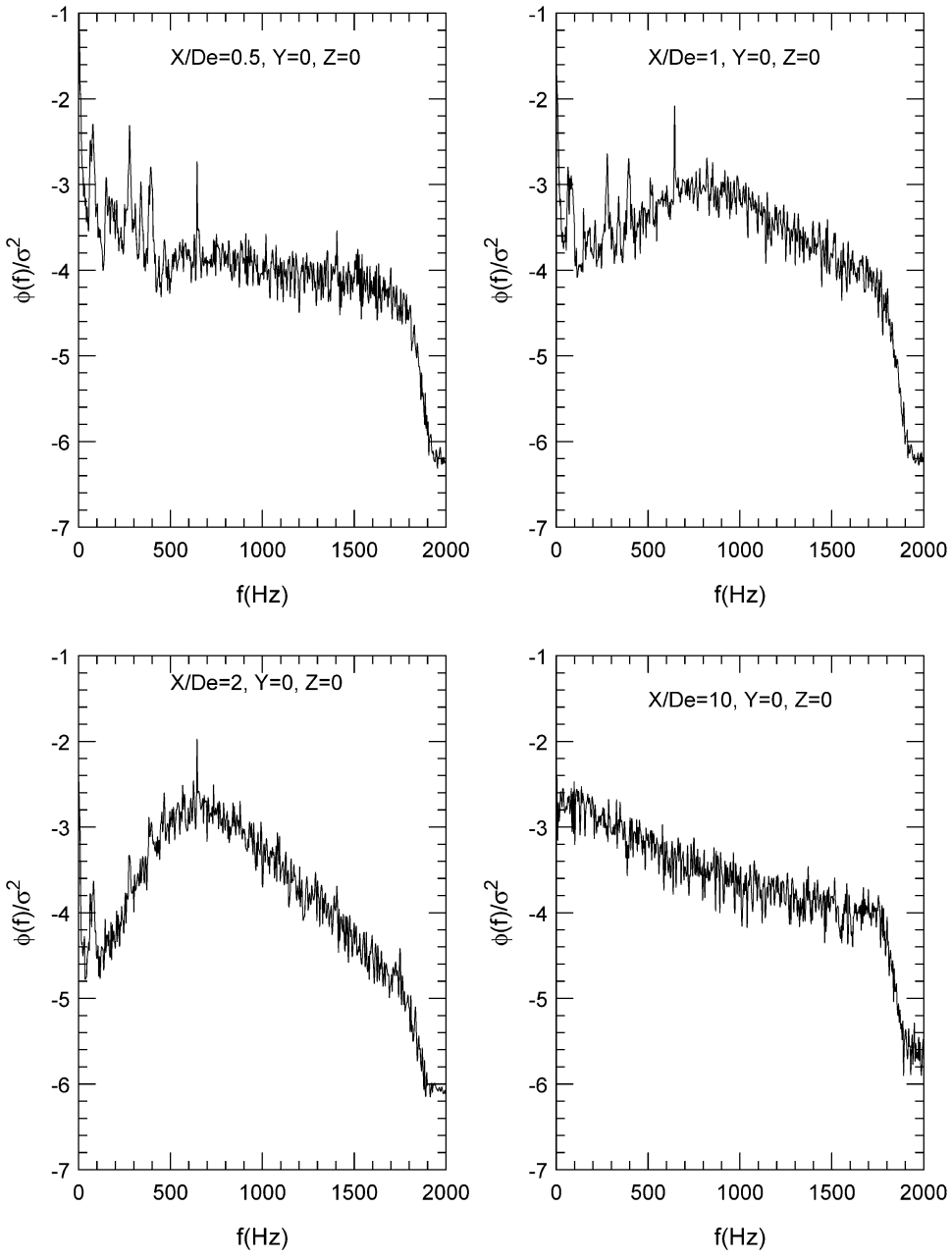

Fig. 17 (*continued*).

The one-dimensional energy spectra results and those of the distribution of the autocorrelation coefficients indicate the presence of large-scale coherent structures in both jets and that these structures are more "energetic" in the sharp-edged orifice jet flow.

Acknowledgements

The support of the Natural Sciences and Engineering Research Council of Canada (NSERC) through research grants awarded to the author and the very helpful comments of the anonymous referees on the original manuscript are gratefully acknowledged.

References

[1] I. Wygnanski, H. Fiedler, Some measurements in the self-preserving jet, J. Fluid Mech. 38 (1969) 577–612.
[2] W. Rodi, A new method of analyzing hot-wire signals in highly turbulent flow, and its evaluation in a round jet, DISA Info 17 (1975) 9–18.
[3] N.R. Panchapasekan, J.L. Lumley, Turbulence measurements in axisymmetric jets of air and helium. Part 1: Air Jet, J. Fluid Mech. 246 (1993) 197–223.
[4] N. Rajaratnam, Turbulent Jets, Elsevier, New York, 1976.
[5] H. Schlichting, Boundary-Layer Theory, McGraw-Hill, New York, 1968.
[6] S. Sami, T. Carmody, H. Rouse, Jet diffusion in the region of flow establishment, J. Fluid Mech. 27 (1967) 231–252.
[7] B.J. Hill, Measurement of local entrainment rate in the initial region of axisymmetric turbulent air jets, J. Fluid Mech. 51 (1972) 773–779.
[8] L. Boguslawski, Cz.O. Popiel, Flow structure of the free round turbulent jet in the initial region, J. Fluid Mech. 90 (1979) 531–539.
[9] N.T. Obot, M.L. Graska, T.A. Trabold, The near field behaviour of round jets at moderate Reynolds numbers, Canad. J. Chem. Engrg. 62 (1984) 587–593.
[10] W.R. Quinn, J. Militzer, Effects of nonparallel exit flow on round turbulent free jets, Int. J. Heat Fluid Flow 10 (2) (1989) 139–145.
[11] J. Mi, G.J. Nathan, D.S. Nobes, Mixing characteristics of axisymmetric free jets from a contoured nozzle, an orifice plate and a pipe, J. Fluids Engrg. 123 (2001) 878–883.
[12] P. Bradshaw, An Introduction to Turbulence and Its Measurement, Pergamon Press, Oxford, 1975.
[13] P.W. Bearman, Corrections for the effect of ambient temperature drift on hot-wire measurements in incompressible flow, DISA Info 11 (11) (1971) 25–30.
[14] J.H. Bell, R.D. Mehta, Three-dimensional structure of plane mixing layers, JIAA Report TR-90, Dept. of Aeronautics and Astronautics, Stanford University, 1989.
[15] T.G. Malmstrom, A.T. Kirkpatrick, B. Christensen, K.D. Knappmiller, Centreline velocity decay measurements in low-velocity axisymmetric jets, J. Fluid Mech. 346 (1997) 363–377.
[16] W.R. Quinn, Streamwise evolution of a square jet cross section, AIAA J. 12 (30) (1992) 2852–2857.
[17] J. Cervantes de Gortari, V.W. Goldschmidt, The apparent flapping motion of a turbulent plane jet – further experimental results, J. Fluids Engrg. 103 (1981) 119–126.
[18] S.C. Crow, F.H. Champagne, Orderly structure in jet turbulence, J. Fluid Mech. 89 (1971) 547–591.
[19] N.W.M. Ko, P.O.A.L. Davies, The near field within the potential cone of subsonic cold jets, J. Fluid Mech. 50 (1971) 49–78.
[20] A.J. Yule, Large-scale structure in the mixing layer of a round jet, J. Fluid Mech. 89 (1978) 413–432.
[21] E. Gutmark, C.-M. Ho, Preferred modes and spreading rates of jets, Phys. Fluids 10 (28) (1983) 2932–2938.
[22] A.K.M.F. Hussain, Coherent structures – reality or myth, Phys. Fluids 26 (1983) 2816–2850.